J Solid State Electrochem (2015) 19:2205–2211
DOI 10.1007/s10008-015-2848-1

ORIGINAL PAPER

Photoelectrochemical characterization of ITO/TiO_2 electrodes obtained by cathodic electrodeposition from aqueous solution

L. F. Marchesi[1,6] · R. G. Freitas[2] · E. R. Spada[3] · F. R. Paula[4] · M. S. Góes[5] · J. R. Garcia[6]

Received: 25 February 2015 / Revised: 30 March 2015 / Accepted: 2 April 2015 / Published online: 22 April 2015

Abstract In the present work, the photoelectrochemical characterization of ITO/TiO_2 electrodes electrosynthesized at two distinct TiO_2 film charges (0.35 and 1.00 C) was performed. Scanning electron microscopy presented a globular-like nanostructure and a typical morphology that are dependent on the growing charge, where the photoelectrode synthesized at 0.35 C presented a more homogeneous morphology. Such dependence was also observed at the photoelectrochemical response, once the photoactivity for the photoelectrode synthesized at 0.35 C was better than the photoelectrode synthesized at 1.00 C, which was explained by the surface recombination process and the electron lifetime. In order to explore the charge-transfer process and the displacement of the quasi-Fermi level upon illumination, electrochemical impedance spectroscopy (EIS) was performed at distinct applied potentials. EIS results corroborate the previous results, presenting a higher charge-transfer resistance and a lower chemical capacitance for the 1.00 C electrode film, the last one in accordance with the open-circuit voltage decay.

Keywords Photoanodes · ITO/TiO_2 electrodes · Cathodic electrodeposition · Electrochemical impedance spectroscopy

✉ J. R. Garcia
jrgarcia@uepg.br

[1] Universidade Tecnológica Federal do Paraná, Av. Monteiro Lobato, s/n Km 04, Ponta Grossa, PR 84016-210, Brazil

[2] GENMAT - Grupo de Eletroquímica e Novos Materiais - Universidade Federal de Mato Grosso, Av. Fernando Corrêa da Costa, 2367, Cuiabá, MT 78060-900, Brazil

[3] Instituto de Física de São Carlos, Universidade de São Paulo, Caixa Posta 369, São Carlos, SP 13560-970, Brazil

[4] Universidade Estadual Paulista "Júlio de Mesquita Filho", Av. Brasil, 56, Ilha Solteira, SP 15385-000, Brazil

[5] Universidade da Integração Latino-Americana, Av. Silvio Américo Sasdelli, 1842, Foz do Iguaçu, PR 85866-000, Brazil

[6] Universidade Estadual de Ponta Grossa, Av. Carlos Cavalcanti, 4748, Ponta Grossa, PR 84030-900, Brazil

Introduction

The search for new materials with a potential applying in renewable and environmentally friendly solar energy devices is the aim of a great number of current papers [1–23]. Among these materials, titanium dioxide (TiO_2) is the subject of recent research [4, 5]. TiO_2 is a *n*-type semiconductor that has, depending on its crystal structure, a band gap energy of 3.2 and 3.0 eV for anatase and rutile phases, respectively, and a range from 3.2 to 3.5 eV in its amorphous state [6–10. Depending on some key redox potentials and the relative position of the TiO_2 band edges, combined with a long electron lifetime in the anatase phase and chemical stability, such material can find numerous functional applications such as gas sensors [11], corrosion resistant coatings [12], photocatalysis [13, 14] and solar energy conversion devices [15, 16].

Considering the abundance of the solar cell energy irradiated at Earth's surface and the amount of available water, the water splitting into H_2/O_2 probably is one the most desired line to support the idea of renewable and environment friendly energy resources. In this way, photocatalytic water splitting using TiO_2 offers a promising way for clean, low-cost, and environmentally friendly H_2/O_2 production. Several papers in the literature have demonstrated that besides the microstructure, the morphology plays an important role in the oxide properties [17, 18]. Yun et al. [19] studied the TiO_2 nanoparticles shape effect on hydrogen production via water splitting. At this study, two shapes were considered, nanospheres and

nanorods, and the authors found that both the charge-transfer rate across the interfacial region and space charge capacitance were significantly improved in the case of nanorods due to a decreased probability of the electron-hole pair recombination, leading to a hydrogen volume generation of 1.6 times for nanorods than nanospheres. Therefore, not only the microstructure and morphology plays an important role in the TiO_2 photocatalytic activity but the synthesis conditions also does. In a recent paper, Freitas et al. [20] prepared TiO_2 nanotubes arrays considering two amounts of ionic liquid, 1 and 5 %wt. The authors found that, besides the similarity in the morphology, crystallite size and band gap values for the obtained TiO_2 nanotubes arrays, a very distinct water-splitting efficiency was observed, that was explained by different electron-hole recombination rate.

One can mention distinct methods to obtain a TiO_2 film, such as sol-gel [21], Pechini [22] and hydrothermal [23]; however, these methods are wet routes, favoring the metastable polymorphs formation (i.e., anatase, brookite), in a ratio that depends on the synthesis variables. In this way, the electrosynthesis (ES) of TiO_2 is an interesting alternative to traditional methods cited above, once such method permits fine-tuning of the synthesis variables, such as current and applied potential [24, 25]. Karuppuchamy et al. [26] prepared crystalline TiO_2 films on several steel substrates by a one-step electrochemical method at low temperature in basic media. Electrodeposition occurred at 60 °C, applying several current densities (from −0.5 to 25 mA/cm^2) at an aqueous solution of 0.1 M of $K_2[TiO(C_2O_4)_2]$ and 1.0 M hydroxylamine, adjusting the pH to 8.0 by addition of KOH. In other study, Karuppuchamy et al. [27] obtained a cathodic electrodeposited ITO/TiO_2 film in acid media applying a constant potential of −1.1 V, at 10 °C, from an aqueous solution containing 0.02 M $TiOSO_4$, 0.03 M H_2O_2, and 0.1 M KNO_3 (pH=1.8). Further heat treatment was necessary to obtain crystalline film in both methods. One can mention that in both works, the resulted TiO_2 structure was well tuned by electrosynthesis.

Considering the exposed above, the main goal of this paper is to promote the photoelectrochemical characterization of the ITO/TiO_2 films grown by cathodic electrodeposition method at two distinct charges, 0.35 and 1.00 C.

Experimental procedure

All reagents were analytical grade.

The morphological characterization was carried out using a Supra 35 Zeiss field emission scanning electron microscope (FESEM).

Electrosynthesis was performed using a conventional three-electrode cell, controlled by an AUTOLAB PGSTA T302N Potentiostat, with a Pt foil as a counter-electrode and a satured calomel electrode (SCE) as a reference. Optically transparent ITO films (Delta Technologies Ltd.) with nominal coating thickness between 150–200 nm and a sheet resistance of 60 Ω/□ (Delta Technologies) were used as a working electrode. The electrolyte was described elsewhere [27], in resume, an aqueous solution containing 0.02 M $TiOSO_4$, 0.03 M H_2O_2, and 0.1 M KNO_3. Electrodeposition occurred at 10 °C by means of an ice-water bath, and the applied potential was −1.1 V vs SCE, varying the total deposited charge, 0.35 and 1.00 C, named, respectively, sample A and sample B. Prior to thermal annealing, samples were dried at room temperature during 24 h. Thermal annealing was performed in a furnace at 600 °C during 2 h, heating the sample at 10 °C/min. After 2 h, the furnace temperature was slowly cooled until reaching room temperature.

After thermal annealing, the resulted thickness was measured using a Veeco DekTak 150 profilometer and it was found values of 110 and 750 nm for samples A and B, respectively.

Photoelectrochemical measurements were performed in a photocell with a quartz window (d=3 cm), using an Autolab PGSTAT-30 Potentiostat/Galvanostat. Platinum wire and ITO/TiO_2 were, respectively, used as counter and working electrodes. All potential were referred to the reversible hydrogen electrode (RHE). Photoelectrochemical test were carried out using a 0.5 M H_2SO_4 solution as electrolyte. A solar simulator (Newport Oriel Arc lamp housing 67005, Oriel xenon lamp 6255, Oriel Arc lamp power supply 69907 USA) was used as a light source.

Electrochemical impedance spectroscopy (EIS) was performed under illumination at several applied *dc* potentials, applying an *ac* potential of 0.010 V in a frequency range from 240 KHz to 30 mHz. Before each EIS measurement, stationary state condition was attained by applying the *dc* potential of interest and waiting constant values of current. The Zview equivalent circuit modeling software (Scribner Associates, North Caroline, USA) was employed for data fitting.

Results

Figure 1 shows the scan electron microscopy images for samples A and B. We can see that the morphology is dependent of the film-deposited charge. Both samples presented a globular-like structure in the range of nanometers that is also dependent of the deposited charge, once for sample A, these nanostructures are smaller than sample B. Besides the similarity in the structure shape, the resulted morphology is quite different for samples A and B. Sample A presents a homogeneous morphology, when compared to sample B. It seems that, at the beginning of the electrodeposition process, a homogeneous film is formed, as we can observe in sample A, recovering all the substrate surface, continuing the electrodeposition, nucleation may occur in some preferred sites, which leads to the

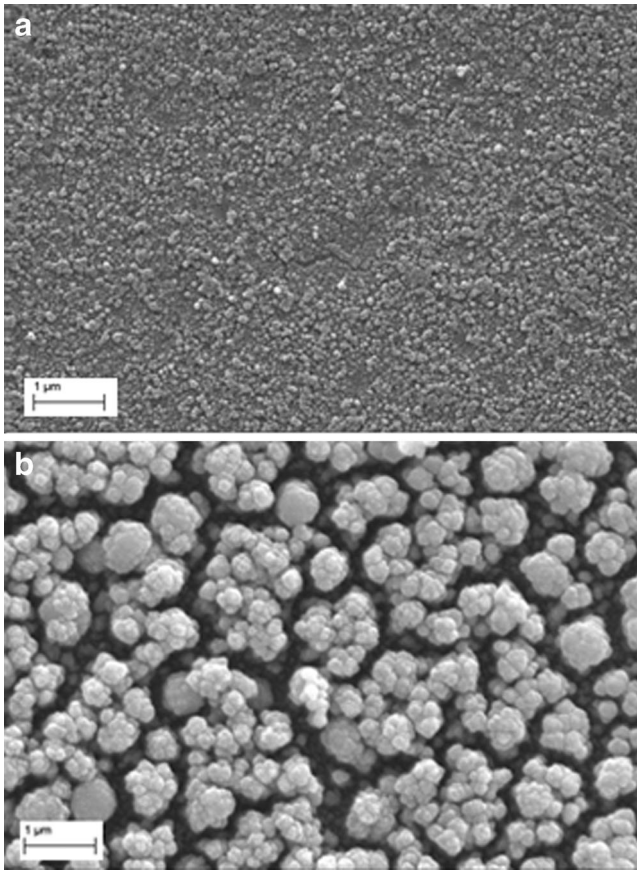

Fig. 1 FESEM images of ITO/TiO_2 electrodes grown in different conditions. **a** Sample A and **b** sample B

formation of clusters which increases the film roughness, as one can see in sample B. Similar behavior was also observed for conducting polymers [28].

Figure 2 shows the photocurrent behavior for the ITO/TiO_2 electrodes over chronoamperograms upon light on/off measurements. One can observe that under illumination, electrons are photogenerated at the TiO_2 film with concomitant transport to the ITO substrate producing a photocurrent. Switching off the light, the recombination between electrons from the TiO_2 conduction band and holes decreases the photocurrent (Fig. 2a). It is interesting to note that both samples present a cathodic current when the light is switched off (Fig. 2b). Such cathodic current is a fingerprint of surface recombination process, which suggests that photogenerated holes are being accumulated in the surface states, increasing the recombination probability and them, decreasing the photocurrent. Interrupting the illumination, such accumulated holes in the surface states continue recombining, originating the cathodic current. Because of the surface recombination, sample B presents a photocurrent lower than sample A, where such process is less pronounced [29, 30].

Figure 3 shows the photocurrent along the UV range. It is possible to observe that the surface recombination process, as discussed above, affects the photocurrent value, presenting

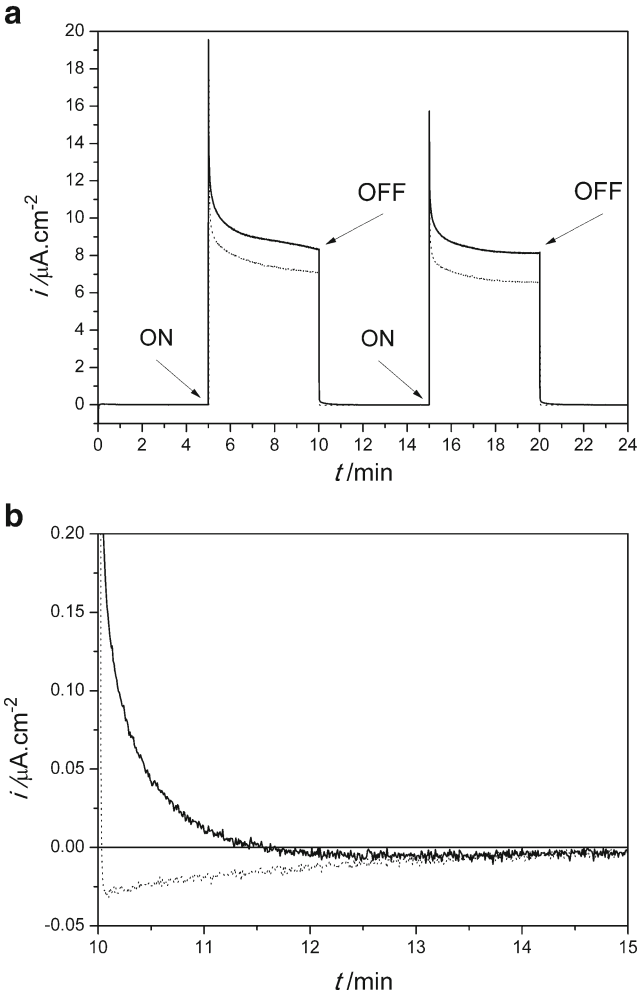

Fig. 2 **a** Photocurrent transients generated during photo irradiation under UV-visible light performed in H_2SO_4 0.5 M electrolyte. **b** Zoomed in photocurrent transients in order to observe the fingerprint of surface recombination process. Sample A (*line*) and sample B (*dot*)

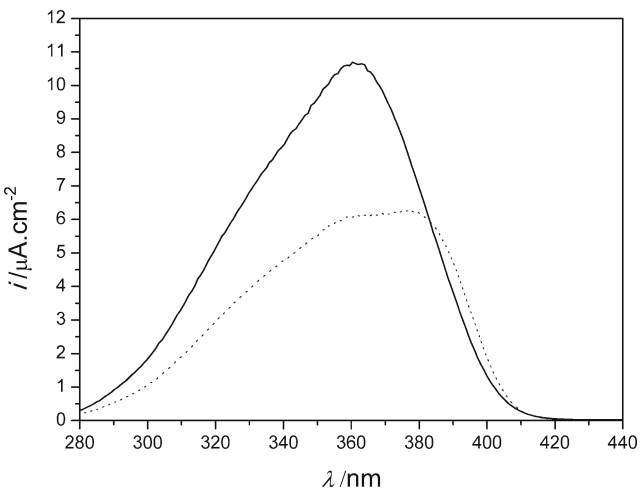

Fig. 3 Photocurrent spectra of the ITO/TiO_2 electrodes performed in H_2SO_4 0.5 M electrolyte. V=0.5 V vs RHE. Sample A (*line*) and sample B (*dot*)

photocurrent values greater for sample A than sample B. One can observe that both samples present a peak wavelength around 360 nm, which is related to the direct inter-band transition originated in TiO_2 particles [31, 32].

A typical open-circuit voltage decay (V_{OC}) response to illumination followed by termination of illumination is showed in Fig. 4a. From 0 to 15 min, at dark conditions, the variation of the *Voc* is due to the stabilization of the double-layer capacitance. The open-circuit voltage of the photoelectrochemical TiO_2 electrodes represents the difference in the Fermi level between the TiO_2 and counter electrodes, which is dictated by redox equilibration in the dark. Band gap excitation of TiO_2 upon illumination results in charge separation, increasing the electron concentration in the TiO_2 film, which causes a shift of the Fermi level to more negative potentials, increasing the V_{OC} [33]. As the electron accumulation occurs, the recombination rate between photogenerated electrons and holes increases, and the open-circuit voltage occurs when the photogeneration and recombination rates are equal, attaining a steady state (region between 15 and 20 min). We can observe that the variation in the voltage upon illumination is more pronounced for sample A (0.63 V) than sample B (0.57 V), indicating a greater variation of the Fermi level for sample A. Switching off the light (after 20 min), no more photogeneration occurs and the accumulated electrons decay upon recombination process, decreasing the open-circuit voltage to a value different from that obtained after the stabilization of the double-layer capacitance. It occurs due to the occupancy of trap states, which increases the Fermi level, increasing the V_{OC} value, as observed. Monitoring such voltage decay can provides an insight into the mechanism loss of accumulated electrons in the TiO_2 film. The V_{OC}-shape curve shows a dependence on the quasi-Fermi level, confirming a trap-assisted conduction mechanism; in other words, it means that not only the free carriers contribute for recombination process but also the charge-transfer, trapping, and detrapping mechanisms [34].

In order to quantify such behavior, Bisquert et al. [34] proposed a model to analyze the electron accumulation decay correlating with the open-circuit voltage decay, as depicted by Eq. (1)]:

$$\tau = \frac{k_B.T}{e}\left(\frac{\partial V_{OC}}{\partial t}\right)^{-1} \quad (1)$$

where k_B is the Boltzmman constant, T the absolute temperature, e the positive elementary charge, and $\partial V_{OC}/\partial t$ the derivative of the open-circuit voltage transient. The resulted electron accumulation decay (τ) applying Eq. (1) to the data in Fig. 4a is shown in Fig. 4b. One can observe that at low voltages, where the photogeneration dominates the recombination process, τ values for sample B are greater than sample A, indicating that the delay in the charge-transfer process is greater in sample B. On the other hand, in voltages near the open-circuit voltage, at around 0.5 V, where the photogeneration and recombination rates are equal, the lifetime for sample A is greater than sample B, indicating that recombination process in sample B is more accentuated. Similar results were observed by Mor et al. [35]. The authors studied highly ordered transparent TiO_2 nanotubes arrays for dye-sensitized solar cell applications and compared such lifetime with TiO_2 nanoparticles one. According to the authors, the transparent TiO_2 nanotubes exhibited longer lifetime, indicating fewer recombination centers in the nanotubular structure. Hossain et al. [36] also observed similar lifetime enhancement for CdSe nanocluster deposited at different times in TiO_2 nanotubes arrays structure.

Photoelectrochemical properties of the TiO_2 film have been examined by evaluating a linear sweep voltammetry (Fig. 5). The linear sweep voltammogram behavior for both samples

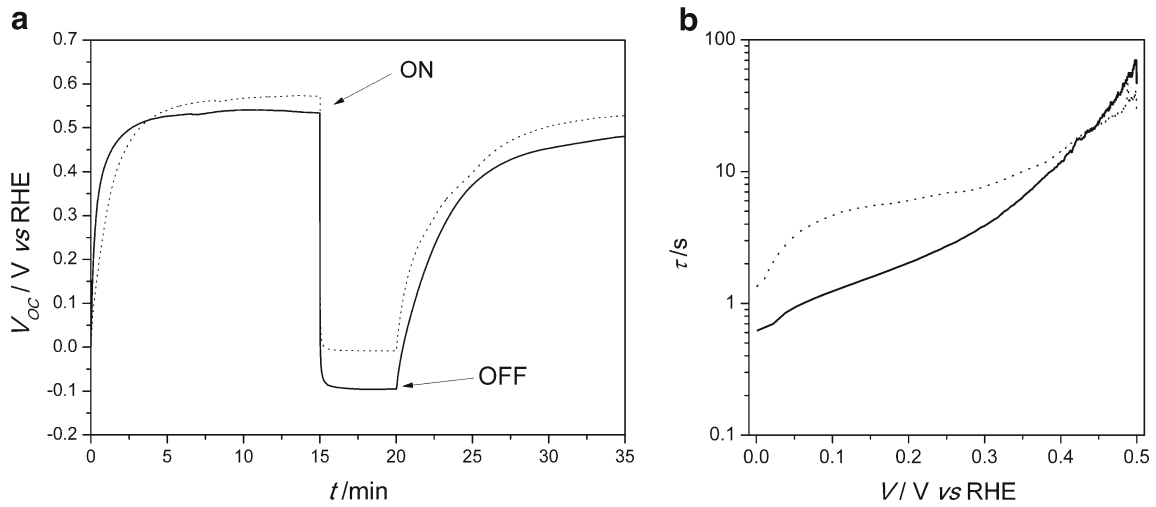

Fig. 4 **a** Open-circuit voltage decay of the ITO/TiO_2 electrodes performed in H_2SO_4 0.5 M electrolyte and **b** electron accumulation decay measurements calculated from the open-circuit voltage decay. Sample A (*line*) and sample B (*dot*)

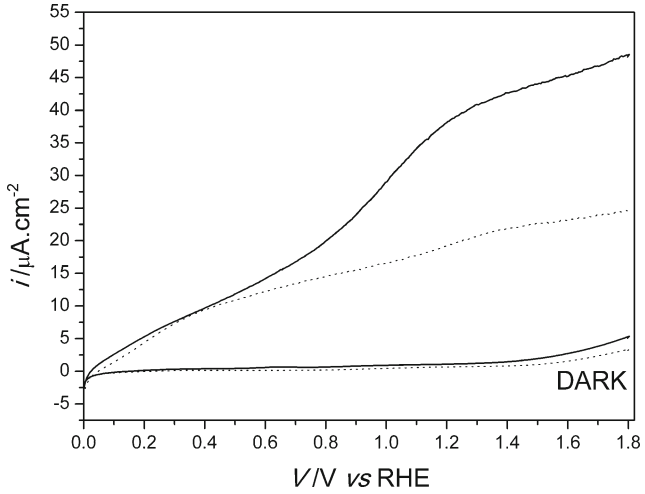

Fig. 5 Linear sweep voltammograms of the ITO/TiO_2 electrodes performed at 50 mV.s^{-1} in H_2SO_4 0.5 M electrolyte. Sample A (*line*) and sample B (*dot*)

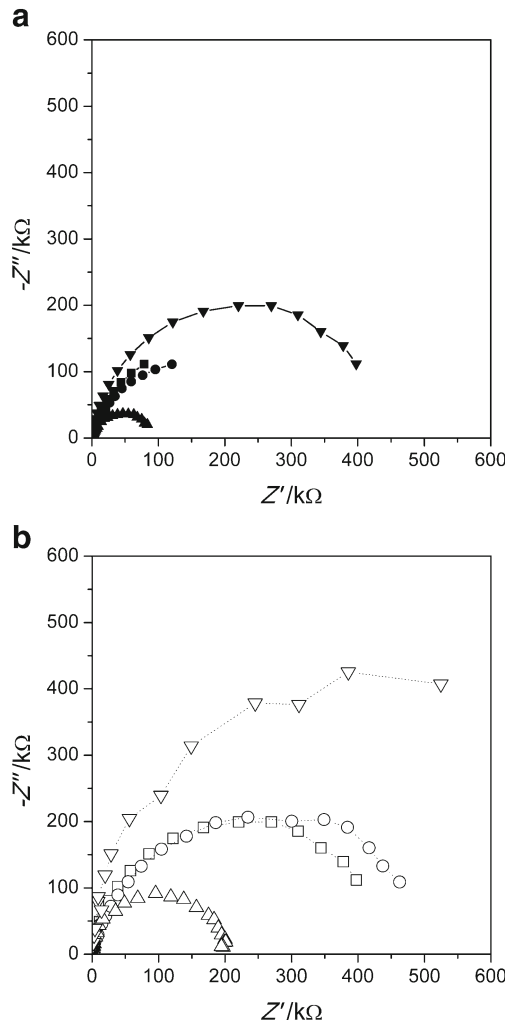

Fig. 6 Nyquist plots of the electrochemical impedance spectroscopy of the ITO/TiO_2 electrodes performed at H_2SO_4 0.5 M electrolyte upon illumination at distinct applied potential. **a** Sample A measured at (▼) 0.1 V, (■) 0.5 V, (●) 1.0 V, and (▲) 1.5 V and **b** sample B measured at (▽) 0.1 V, (□) 0.5 V, (○) 1.0 V, and (Δ) 1.5 V

shows a typical behavior of *n*-TiO_2 semiconductor, presenting a positive relationship between the photocurrent and the applied potential, and almost reaching a plateau-like behavior at 1.4 V for samples A and B. One can observe that sample A presents a photocurrent greater than sample B, in order of 190 %, comparing the peak photocurrent. Dark response was also shown in order to verify that no leakage of current was present.

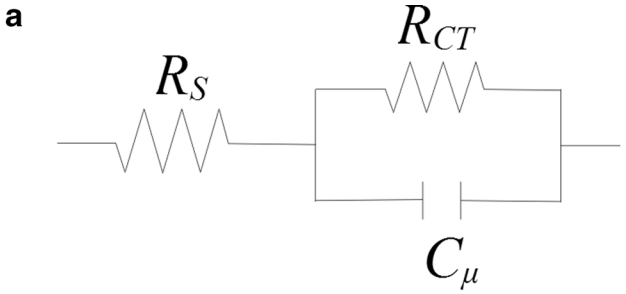

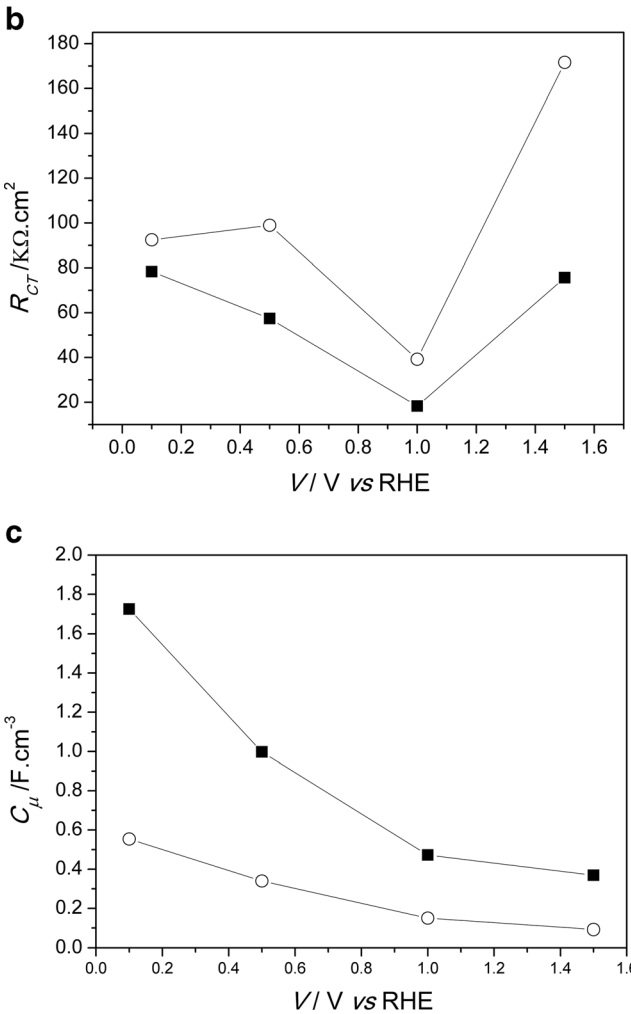

Fig. 7 **a** Equivalent circuit model used to fit EIS data presented in Fig. 6. R_S is the series resistance, R_{CT} the charge-transfer resistance, and C_μ the chemical capacitance. **b** Charge-transfer resistance as a function of the applied potential for (■) sample A and (○) sample B. **c** Chemical capacitance as a function of the applied potential for (■) sample A and (○) sample B

Figure 6 shows the EIS response for samples A and B as a function of the applied potential. For both samples, we can observe the same behavior, one potential-dependent semicircle, which is related to the charge-transfer resistance, associated to the oxygen evolution reaction, combined with the chemical capacitance (C_μ) [37]. The EIS data were fitted using the appropriate equivalent circuit model, as showed in Fig. 7a, consisting of a series resistance (R_S), accounting for the electrolyte and contacts contribution, a resistance accounting for the charge-transfer resistance (R_{CT}) and a capacitance accounting for the chemical capacitance (C_μ). In order to compare R_{CT} and C_μ for samples A and B, such values were normalized by geometric area and film volume, respectively [38, 39].

Figure 7b presents the charge-transfer resistance (R_{CT}) as a function of the applied potential for both samples. The behavior presented in both samples is typical of charge transfer via surface state, as discussed elsewhere [40], in accordance with the results presented in Fig. 2. The R_{CT} values are greater for sample B, indicating that the charge-transfer process accounting for the oxygen evolution is more facilitate in sample A, supporting the greater values of photocurrent encountered in such sample (Fig. 5).

The chemical capacitance (C_μ) as a function of the applied potential is showed in Fig. 7c. One can observe that the values for sample A are greater than sample B. As described above, the C_μ relates the quasi-Fermi level displacement upon illumination, showing that the displacement for sample A is more pronounced than sample B, which confirms the V_{OC} measurements (Fig. 4a), where we can observe that the voltage variation upon darkness and illumination is also more pronounced for sample A.

Conclusions

In this paper, the photoelectrochemical characterization of the ITO/TiO_2 electrodes synthesized by electrochemical methods at two distinct growing charges was performed (0.35 and 1.00 C, named, respectively, sample A and sample B). Besides the morphology, the growing charge also determined the electrodes photoactivity, where sample A presented the best results. The typical surface recombination process showed in the photocurrent transients generated during photoirradiation under UV-visible light was the main drawback in the performance of sample B, where such process was more pronounced, which was confirmed by the electrochemical impedance spectroscopy, where sample A presented the lowest values of the charge-transfer resistance. Moreover, the chemical capacitance values were greater for sample A, indicating that the displacement of the quasi-Fermi level for such electrode is more pronounced, which was also confirmed by the open-circuit voltage decay measurement.

Acknowledgments The authors should thank the financial support from Conselho Nacional de Desenvolvimento Científico e Tecnológico (CNPq) under Universal Project (446320/2014-5) and Scholarship (158984/2014-5), the National Institute for Science and Technology on Organic Electronics (INEO), Fundação de Amparo à Pesquisa do Estado de São Paulo (FAPESP), and Fundação Araucária do Estado do Paraná.

References

1. Omata T, Nagatani H, Suzuki I, Kita M, Yanagi H, Ohashi N (2014) Wurtzite $CuGaO_2$: a new direct and narrow band gap oxide semiconductor applicable as a solar cell absorber. J Am Chem Soc 136: 3378–3381
2. Behrouznejad F, Taghavinia N (2014) High-performance/low-temperature-processed dye solar cell counter electrodes based on chromium substrates with cube-like morphology. J Power Sources 260: 299–306
3. Gupta A, Vashistha M, Sharma P (2014) Single junctions a-Si:H solar cell with a-Si:H/nc-Si:H/a-Si:H quantum wells. Thin Solid Films 550:643–648
4. Hu S, Shaner MR, Beardslee JA, Lichterman M, Brunschwig BS, Lewis NS (2014) Amorphous TiO_2 coatings stabilize Si, GaAs, and GaP photoanodes for efficient water oxidation. Science 344:1005–1009
5. Lu X, Yang W, Quan Z, Lin T, Bai L, Wang L, Huang F, Zhao Y (2014) Enhanced electron transport in Nb-doped TiO_2 nanoparticles via pressure-induced phase transitions. J Am Chem Soc 136: 419–426
6. Gai Y, Li J, Li SS, Xia JB, Wei SH (2009) Design of narrow-gap TiO_2: a passivated codoping approach for enhanced photoelectrochemical activity. Phys Rev Lett 102:036402
7. Long R, English NJ (2009) First-principles calculation of nitrogen-tungsten codoping effects on the band structure of anatase-titania. Appl Phys Lett 94:132102
8. Preclíková J, Galár P, Trojánek F, Rezek B, Nemcová Y, Malý P (2011) Photoluminescence of nanocrystalline titanium dioxide films loaded with silver nanoparticles. J Appl Phys 109:083528
9. Hari M, Joseph SA, Mathew S, Radhakrishnan P, Nampoori VPN (2012) Band-gap tuning and nonlinear optical characterization of Ag: TiO_2 nanocomposites. J Appl Phys 112:074307
10. Eufinger K, Poelman D, Poelman H, De Gryse R, Marin GB (2007) Photocatalytic activity of dc magnetron sputter deposited amorphous TiO_2 thin films. Appl Surf Sci 254:148–152
11. Nisar J, Topalian Z, De Sarkar A, Osterlund L, Ahuja R (2013) TiO_2-based gas sensor: a possible application to SO_2. ACS Appl Mater Interfaces 5:8516–8522
12. Baghery P, Farzam M, Mousavi AB, Hosseini M (2010) Ni-TiO_2 nanocomposite coating with high resistance to corrosion and wear. Surf Coat Technol 204:3804–3810
13. Xu H, Ouyang S, Liu L, Reunchan P, Umezawa N, Ye J (2014) Recent advances in TiO_2-based photocatalysis. J Mater Chem A 2: 12642–12661
14. Xu C, Yang W, Guo Q, Dai D, Chen M, Yang X (2014) Molecular hydrogen formation from photocatalysis of methanol on anatase-TiO_2 (101). J Am Chem Soc 136:602–605
15. Wang JTW, Ball JM, Barea EM, Abate A, Alexander-Webber JA, Huang J, Saliba M, Mora-Sero I, Bisquert J, Snaith HJ, Nicholas RJ (2014) Low-temperature processed electron collection layers of graphene/tio_2 nanocomposites in thin film perovskite solar cells. Nano Lett 14:724–730
16. Roiati V, Mosconi E, Listori A, Colella S, Gigli G, De Angelis F (2014) Stark effect in perovskite/tio_2 solar cells: evidence of local interfacial order. Nano Lett 14:2168–2174

17. Babu VJ, Kumar MK, Nair AS, Kheng TL, Allakhverdiev SI, Ramakrishna S (2012) Visible light photocatalytic water splitting for hydrogen production from N-TiO2 rice grain shaped electrospun nanostructures. Int J Hydrogen Energy 37:8897–8904
18. Li Y, Yu H, Zhang C, Song W, Li G, Shao Z, Yi B (2013) Effect of water and annealing temperature of anodized TiO_2 nanotubes on hydrogen production in photoelectrochemical cell. Electrochem Acta 107:313–319
19. Yun HJ, Lee H, Joo JB, Kim ND, Yi J (2011) Effect of TiO_2 nanoparticles shape on hydrogen evolution via water splitting. J Nanosci Nanotechno 11:1–4
20. Freitas RG, Santanna MA, Pereira EC (2014) Preparation and characterization of TiO_2 nanotube arrays in ionic liquid for water splitting. Electrochem Acta 136:404–411
21. Hartmann P, Lee DK, Smarsly BM, Janek J (2010) Mesoporous TiO_2: comparison of classical sol-gel and nanoparticle based photoelectrodes for the water splitting reaction. ACS Nano 4: 3147–3154
22. Drev M, Krasovec UO, Hocevar M, Berginc M, Macek MK, Topic M (2011) Pechini based titanium sol as a matrix in TiO_2 pastes for dye-sensitized solar cell applications. J Sol-Gel Sci Technol 59: 245–251
23. Phan TDN, Pham HD, Cuong TV, Kim EJ, Kim S, Shin EW (2009) A simple hydrothermal preparation of TiO_2 nanomaterials using concentrated hydrochloric acid. J Cryst Growth 312:79–85
24. Silva NR, Cid CCP, Spada ER, Reis FT, Faria RM, Sartorelli ML (2014) Electrosynthesized TiO2 films: dependence of the brookite-anatase ratio on the applied potential. J Mater Sci 49:2952–2959
25. Campos CS, Spada ER, Paula FR, Reis FT, Faria RM, Sartorelli ML (2012) Raman and XRD study on brookite-anatase coexistence in cathodic electrosynthesized titania. J Raman Spectrosc 43:433–438
26. Karuppuchamy S, Suzuki N, Ito S, Endo T (2009) A novel one-step electrochemical method to obtain crystalline titanium dioxide films at low temperature. Curr Appl Phys 9:243–248
27. Karuppuchamy S, Nonomura K, Yoshida T, Sugiura T, Minoura H (2002) Cathodic electrodeposition of oxide semiconductor thin films and their application to dye-sensitized solar cells. Solid State Ionics 151:19–27
28. Garcia-Blemonte G, Bisquert J (2002) Impedance analysis of galvanostatically synthesized polypyrrole films. Correlation of ionic diffusion and capacitance parameters with the electrode morphology. Electrochim Acta 47:4263–4272
29. Abrantes LM, Peter LM (1983) Transient photocurrents at passive iron electrodes. J Electroanal Chem Interfacial Electrochem 150: 593–601
30. Peter LM (1990) Dynamic aspects of semiconductor photoelectrochemistry. Chem Rev 90:753–769
31. Luo J, Huang HG, Zhang HP, Wu LL, Lin ZH, Hepel M (2000) Studies on photoelectrochemistry of nano-particulate TiO_2/PANI/PATP film on Au electrodes. J New Mat Electr Sys 3:249–252
32. Solarska R, Rutkowska I, Augustynski J (2008) Unusual photoelectrochemical behaviour of nanocrystalline TiO_2 films. Inorg Chim Acta 361:792–797
33. Meekins BH, Kamat PV (2009) Got TiO_2 nanotubes? Lithium ion intercalation can boost their photoelectrochemical performance. ACS Nano 3:3437–3446
34. Bisquert J, Zaban A, Greenshtein M, Mora-Seró I (2004) Determination of rate constants for charge transfer and the distribution of semiconductor and electrolyte electronic energy levels in dye-sensitized solar cells by open-circuit photovoltage decay method. J Am Chem Soc 126:13550–13559
35. Mor GK, Shankar K, Paulose M, Varghese OK, Grimes CA (2006) Use of highly-ordered TiO_2 nanotube arrays in dye-sensitized solar cells. Nano Lett 6:215–218
36. Hossain MF, Biswas S, Zhang ZH, Takahashi T (2011) Bubble-like CdSe nanoclusters sensitized TiO_2 nanotube arrays for improvement in solar cell. J Photochem Photobiol A 217:68–75
37. Gimenez S, Dunn HK, Rodenas P, Fabregat-Santiago F, Miralles SG, Barea EM, Trevisan R, Guerrero A, Bisquert J (2012) Carrier density and interfacial kinetics of mesoporous TiO_2 in aqueous electrolyte determined by impedance spectroscopy. J Electroanal Chem 668:119–125
38. Marchesi LF, Pereira EC (2014) The influence of the drying process on electrochemical properties of P3HT/PCBM (1.00/0.25 wt%) electrodes. Synth Met 194:82–87
39. Fabregat-Santiago F, Barea EM, Bisquert J, Mor GK, Shankar K, Grimes CA (2008) High carrier density and capacitance in TiO_2 nanotube arrays induced by electrochemical doping. J Am Chem Soc 130:11312–11316
40. Mora-Seró I, Bisquert J (2003) Fermi level of surface states in TiO_2 nanoparticles. Nano Lett 3:945–949